Relativistic close-coupling calculation of photoionization and photorecombination of Fe XVI

Guo-Xin Chen
ITAMP, Harvard-Smithsonian Center for Astrophysics, 60 Garden Street, Cambridge, Massachusetts 02138, USA
(Received 17 July 2007; revised manuscript received 25 November 2007; published 5 February 2008)

Large-scale relativistic close-coupling calculation of photoionization and photorecombination of Fe XVI reveal strong resonance structures at low energies. The Breit-Pauli *R*-matrix method was employed in the calculations with the inclusion of 89 spectroscopic states in the close-coupling eigenfunction expansion. Our unified photorecombination cross sections show significant differences from previous results. The Gaussian averaged effective photorecombination cross sections to the $2p^6 3d_{3/2,5/2}$ states of Fe XVI are shown to be 24% larger than those used for normalization by Brown *et al.* [Phys. Rev. Lett. **96**, 253201 (2006)]. This result should help resolve the issue raised in Brown's paper on the puzzling large discrepancy between theoretical and experimental electron impact excitation cross sections of Fe XVII.

DOI: 10.1103/PhysRevA.77.022703 PACS number(s): 32.80.Fb, 34.80.Lx

I. INTRODUCTION

Photoionization (PI) and photorecombination (PR) of atomic ions are fundamental atomic processes important for the study of astrophysical, fusion, and laser-produced plasmas [1–3]. Along with other radiative and collisional atomic processes, accurate calculations of cross sections and rates for these atomic processes are essential for theoretical modeling and diagnostics of plasmas, such as the accurate determination of level populations and element abundances [4–6] in astrophysical plasmas of photoionized equilibrium or collisionally ionized equilibrium appearing in solar and stellar coronae, active galactic nuclei, supernovae, and black holes [7,8]. Very recently and more interestingly, the need for accurate PR cross sections and rates is also compelling in the modeling of electron beam ion trap (EBIT) x-ray spectrum measurements [9,10]. As a typical case study shown in a recent paper [10], Brown *et al.* argue that they have established a benchmark for atomic calculations of Fe XVII. The method they used is to measure the absolute electron impact excitation (EIE) cross sections of x-ray transitions 3C (λ15.015 Å) and 3D (λ15.262 Å) in Fe XVII when normalizing the 3C and 3D spectrum to the weak radiative recombination (RR) spectrum.

The determination of accurate EIE cross sections in Fe XVII plays a cornerstone role in the field of x-ray astrophysics [10–15]. The ground electronic configuration of Fe XVII has a stable closed *L*-shell structure, rendering Fe XVII the dominant Fe ion species in a wide range of astrophysical plasmas [11,7]. Therefore, the intensity ratios of Fe XVII x-ray lines in the soft x-ray region ~10–17 Å can be used as a fundamental diagnostic tool to reveal the nature of astrophysical sources, such as high-temperature stellar coronae and accretion disks around active galactic nuclei given that the line formation mechanisms in Fe XVII are well studied and can be accurately modeled [5,10,14,15]. The accuracy of EIE cross sections in Fe XVII reported in [10] depends critically on the theoretical recombination rates of Fe XVI. However, a relativistic Hartree-Slater (RHS) model was used in [10] to calculate the recombination cross sections [16,17]. It is therefore compelling to verify the cross sections used in [10] for recombination to the ground state and in particular to the excited states (such as $3d_{3/2,5/2}$) of Fe XVI by employing the advanced relativistic close-coupling method. There are only a limited number of theory calculations on the PI of Fe XVI in the literature (e.g., [19]), and they are mainly for the ground 3*s* state or the inner shell PI. More importantly, to the author's knowledge, so far no accurate Breit-Pauli *R*-matrix (BPRM) calculation has been carried out for the unified photorecombination to the 3*d* excited states of Fe XVI.

II. METHOD AND CALCULATION

The relativistic close-coupling calculation of photoionization of Fe XVI was carried out using the advanced Breit-Pauli *R*-matrix method [18]. In order to explore the extensive resonance structures in PI and PR of Fe XVI, we included many Rydberg series of resonances converging on to a number of $n=3$ and $n=4$ Fe XVII target levels. Many infinite and interacting series of resonances arise due to coupling between open and closed scattering channels which, in principle, must be included in order to obtain the cross sections precisely. But for a complex ion such as Fe XVI the number of channels is very large and the close-coupling (CC) calculations are challenging especially when relativistic fine structure is also considered in addition to other atomic effects. The coupled-channel wave-function expansion for the (e+Fe XVII) system is expressed as

$$\Psi(E;e+\text{Fe XVII}) = \sum \chi_i(\text{Fe XVII})\theta_e(\ell_i) + \sum c_j \Phi_j(\text{Fe XVI}), \quad (2.1)$$

where the functions Ψ denote the continuum states ($E>0$) for given total angular momentum and parity $J\pi$, expanded in terms of the core ion eigenfunctions $\chi_i(S_iL_iJ_i)$, the free-electron partial wave $\theta_e(\ell_i)$, and the bound channels Φ_j which serve as short-range correlation functions and also compensate for orthogonality constraints.

The calculation was carried out using the BPRM method [18] with a large eigenfunction expansion including 89 spectroscopic fine-structure levels corresponding to 49 *LS* terms up to the $n=3$ (n is the principal quantum number) and the $n=4$ complexes of Fe XVII. These 89 spectroscopic levels

 ©2008 The American Physical Society

belong to 15 configurations $2s^22p^6$, $2s^22p^5(3s,3p,3d)$, $2s^22p^5(4s,4p,4d,4f)$, $2s^12p^6(3s,3p,3d)$, and $2s^12p^6(4s,4p,4d,4f)$. A few pseudostates were also included to improve the target quality. We consider total symmetries $2J \leq 7$ for odd parity and $2J \leq 5$ for even parity explicitly in the BPRM calculations. The dimension of Hamiltonian matrices ranges up to 6029, for $2J=7$ with 392 free channels and 149 bound channels (Φ_j). Fifteen continuum basis functions are used to represent the $\Psi(e+\text{Fe XVII})$ in the inner R-matrix region. Particular attention is paid to the resolution of resonances, with cross sections computed at about 12 000 energies.

The PR processes were treated within the framework of the unified theoretical approach for both the RR and dielectronic recombination (DR). The PR cross sections were calculated from the BPRM PI cross section via the Milne detailed balance [20–22]. This method has been benchmarked by a number of calculations to within the experimental uncertainties, for example, in our previous PR calculation of $(e+C\ \text{IV})$ [23]. Traditionally recombination processes are divided separately into two types: RR and DR. In the RR process, an incident electron is combined with the target ion through the nonresonant background continuum, which is the inverse process of direct PI. In the DR process, an incident electron is combined with the target ion through a two-step recombination process via autoionizing resonances, where the incident electron is in a quasibound doubly excited state, which further leads either to (i) autoionization, a radiationless transition to a lower state of the ion and a free electron; or to (ii) radiative stabilization predominantly via decay of the ion core and a bound electron. The incoming electron may be recombined into an infinite number of Rydberg series converging onto an infinite number of target levels.

The two recombination processes RR and DR are unified in nature, so both RR and DR should be treated coherently. The BPRM close-coupling calculations for PI cross sections σ_{PI} include both background and resonance structures (due to the doubly excited autoionizing states) in the cross sections. In the unified method the PR cross section σ_{PR} is related to the BPRM PI cross sections σ_{PI} through the generalized principle of detailed balance (Milne relation) as [21,22]

$$\sigma_{\text{PR}}(E) = \frac{\alpha^2}{4}\frac{g_i}{g_j}\frac{\omega^2}{E}\sigma_{\text{PI}}(E), \tag{2.2}$$

where E is the photoelectron energy and ω is the photon energy. g_i and g_j are the statistical weights for the initial state of the recombined ion and the final state of the recombining ion, respectively. α is the fine-structure constant.

III. RESULTS

A. Detailed PI and PR cross sections

Figures 1(a) and 1(b) show the detailed cross sections of the partial photoionization ($h\nu$+Fe XVI) from the Fe XVI specific fine-structure levels $3d_{3/2}$ and $3d_{5/3}$, respectively, leaving the core ion Fe XVII in the ground state. The photoelectron energy range 50–80 Ry (corresponding to photon energy range 80–110 Ry) shown in Fig. 1 is chosen to be of interest

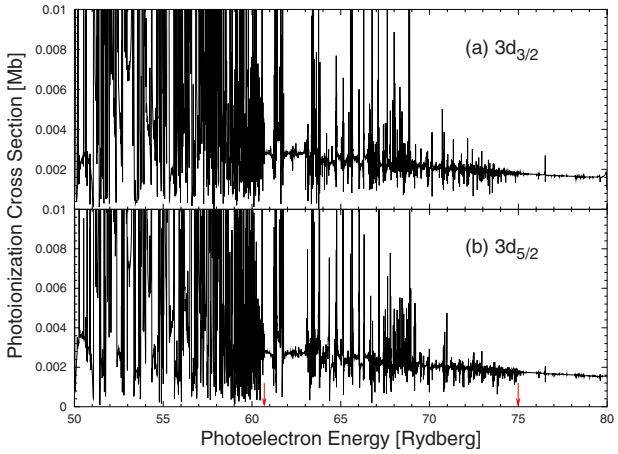

FIG. 1. (Color online) Detailed fine-structure photoionization cross sections σ_{PI} as a function of photoelectron energy from Fe XVI state (Ne core) $3d_{3/2}$ [top panel (a)] and $3d_{5/2}$ [bottom panel (b)]. The two downward arrows mark the highest target thresholds of $n=3$ and 4 complexes (excitation from the $2p^6$ subshell), respectively.

also in the theoretical and experimental study of low-energy EIE processes in Fe XVII [14,10]. At low photoelectron energy, series of prominent and dense Rydberg resonances converge onto the Fe XVII target states up to $2p^53d$ thresholds, as shown in Fig. 1.

Using the generalized principle of detailed balance (Milne relation) described in Eq. (2.2), the unified recombination cross sections (RR+DR) can be calculated from the detailed PI cross sections in Fig. 1. The unified photorecombination (RR+DR) cross sections to the Fe XVI specific fine-structure levels $3d_{3/2}$ and $3d_{5/3}$ are shown in Figs. 2(a) and 2(b), respectively. Figure 2(c) shows the sum of the unified recombination cross sections in Figs. 2(a) and 2(b) for PR to the two $2p^63d$ fine-structure states. The DR and the interference

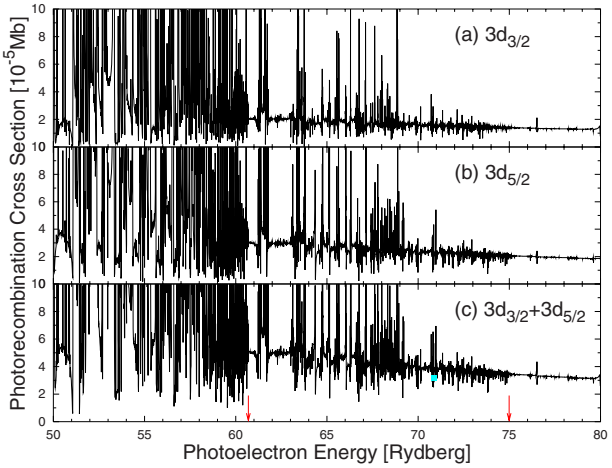

FIG. 2. (Color online) Detailed fine-structure photocombination cross sections σ_{PR} as a function of photoelectron energy to Fe XVI state (Ne core) $3d_{3/2}$ [top panel (a)], $3d_{5/2}$ [middle panel (b)], and the sum of both the $3d_{3/2}$ and $3d_{5/2}$ states [bottom panel (c)]. The square in panel (c) is the previous RHS RR result given in [10].

of RR and DR are clearly demonstrated at low energy in Fig. 2. The previous RHS theory result from [10] is shown as a square in Fig. 2(c). From the comparison of Fig. 2(c), the previous RHS RR data from [10] is about 24% smaller than the present background recombination value (mainly RR cross section). The data in Fig. 2(c) may also be used to reanalyze the measured spectrum reported in [10] when the detailed cross sections are convolved with the electron beam spread assumed to be a Gaussian $g(E)$ [24] (discussed below). The line profile of the RR emission in EBIT measurements is described as a Gaussian function due to the electron beam spread [24].

B. Line intensity and effective cross sections

Next, as a major motivation in this work, we apply the theoretical recombination results in Fig. 2 to reanalyze the experimental spectrum measured by EBIT [10]. The intensity of dipole radiation line 3C I_{3C} of Fe XVII (due mainly to EIE) can be expressed as [14,15,10]

$$I_{3C} = \eta_{3C} \int g(E) v_e dE \bar{\sigma}_{3C} n_e n_{\text{Fe XVII}}, \tag{3.1}$$

where n_e and $n_{\text{Fe XVII}}$ are the electron density and the Fe XVII ion density, respectively. η_{3C} is the combined correction coefficient for the detector. v_e is the velocity of the incident electron. $\bar{\sigma}_{3C}$ is the 3C EIE effective cross section [14]. The determination of EIE cross sections is the theme of [10]. The 3C EIE effective cross sections may be obtained by the approach of normalizing the 3C line intensity to the line intensity of weak recombination line I_{PR}, which is expressed as

$$I_{PR} = \eta_{PR} \int g(E) v_e dE \bar{\sigma}_{PR} n_e n_{\text{Fe XVII}}. \tag{3.2}$$

Here the effective photorecombination cross section $\bar{\sigma}_{PR}$ is defined as

$$\bar{\sigma}_{PR} = \frac{\int \sigma_{PR}(E) g(E) v_e dE}{\int g(E) v_e dE}, \tag{3.3}$$

where $g(E)$ is the electron beam distribution of EBIT assumed to be a Gaussian distribution function. $\bar{\sigma}_{PR}$ can be readily calculated from the unified PR cross section σ_{PR} shown in Fig. 2. From Eqs. (3.1) and (3.2), the 3C EIE effective cross section $\bar{\sigma}_{3C}$ may then be obtained,

$$\bar{\sigma}_{3C} = (\eta_{PR}/\eta_{3C}) \bar{\sigma}_{PR} \frac{I_{3C}}{I_{PR}}. \tag{3.4}$$

In Table I, we calculated the effective PR cross section $\bar{\sigma}_{PR}$ from Eq. (3.3) at four electron beam energies E_0 =900–994 eV and three electron beam spreads with full width at half-maximum (FWHM) W=10, 20, and 50 eV. The present $\bar{\sigma}_{PR}=3.92\times10^{-5}$ Mb at E_0=964 eV and W=20 eV is 24% larger than the data 3.16×10^{-5} Mb calculated with the RHS method and used in [10]. We note that at E_0=934 eV, $\bar{\sigma}_{PR}=4.47\times10^{-5}$ Mb for W=10 eV is even larger than $\bar{\sigma}_{PR}$ for both W=20 and 50 eV. This point reflects the local resonance structures in the detailed PR cross sections in Fig. 2, which is also the source for the oscillation behavior of $\bar{\sigma}_{PR}$ at smaller FWHM (see discussion in Fig. 3). In Fig. 3, $\bar{\sigma}_{PR}$ is further plotted against the electron beam energy for three different beam spreads: W=10 eV (red curve with small oscillations), W=20 eV (black curve), and W=50 eV (green curve with a sharp increase at low energy). The previous RHS RR data are shown as a square in Fig. 3. The sheer increase of $\bar{\sigma}_{PR}$ (significantly deviated from the RR behavior) at low energy is due to DR and the interference of RR and DR as explained and demonstrated in Fig. 2. The sheer increase in the green curve for W=50 eV appears at higher electron beam energy because with larger FWHM the effective PR cross sections are obtained with the Gaussian distribution that may overlap the resonance region at lower energy where prominent DR and the interference of DR+RR show up as expected. The red curve for W=10 eV shows small but discernible oscillations in the effective PR cross sections just below 70 Ry. Much more prominent oscillations will show up at lower electron energy or smaller beam spread as we may also expect.

TABLE I. Effective photorecombination cross sections $\bar{\sigma}_{PR}$ (in units 10^{-23} cm^2=10^{-5} Mb) for the sum of both the $3d_{3/2,5/2}$ states calculated from the present BPRM calculations are compared with previous RR calculation by the RHS model.

E	Present BPRM			RHS [10]
	W=10 eV	20 eV	50 eV	
900 eV	4.80	4.83	5.70	
934 eV	4.47	4.36	4.45	
964 eV	3.89	3.92	4.01	3.16[a]
994 eV	3.63	3.64	3.70	

[a] $\sigma_{RR}=[\sigma_{RR}(\text{at } 90°)]\times\frac{3-P}{3}$, where P=0.57 given in [10] is the linear polarization of the emitter RR radiation.

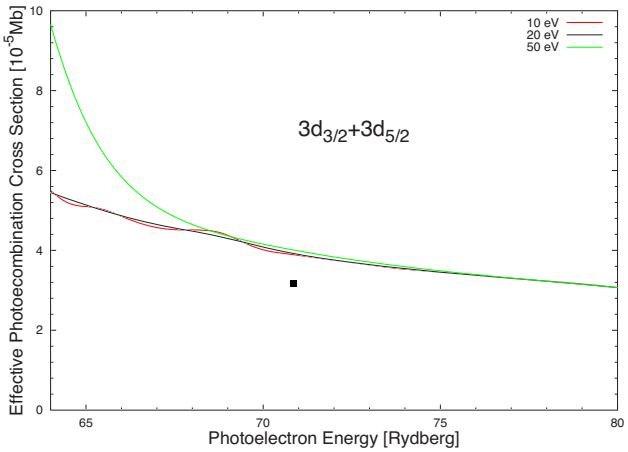

FIG. 3. (Color online) Effective photorecombination cross sections $\bar{\sigma}_{PR}$ [sum of both Fe XVI states (Ne core) $3d_{3/2,5/2}$] as a function of photoelectron energy convolved with a Gaussian distribution of FWHM W=10 eV (red line with small oscillations), W=20 eV (black line), and W=50 eV (green line with a sheer increase at low energy). The square is the previous RHS RR result given in [10].

From Eq. (3.4), because the more elaborate BPRM method than the previous RHS approach was used in our calculation, the present, more accurate, theoretical $\bar{\sigma}_{PR}$ value (24% larger than the RHS data) will naturally result in a 24% increase in $\bar{\sigma}_{3C}$ compared to those presented in Tables I and II and Fig. 2 in [10] if the same EBIT spectrum measurement is used to obtain I_{3C} and I_{PR}. This result reduces significantly the puzzling large discrepancy (up to 50% or more) between the Fe XVII 3C and 3D EIE cross sections obtained by earlier theoretical calculations and those derived in [10]. The limitation of the Hartree-Slater model for the subshell photoionization calculations and the corresponding subshell photorecombination calculations via the principle of detailed balance has been pointed out in Ref. [16], but it may not be fully aware in some recent works such as [10,24]. The EIE cross sections for the 3C and 3D lines derived in [10] should also be called effective cross sections instead of the absolute cross section because the convolution of electron beam distribution needs to be first performed and the cascade effects cannot be easily discerned, in addition to the fact that there is some significant uncertainty in the recombination cross section in [10] as we have already discussed above. It should also be noted that radiation damping (RD) effect was included in our calculations of PI and PR processes. This RD effect is found to be negligibly small in particular for the photoelectron energy range of 900–1000 eV needed to analyze the EBIT spectrum in [10]. The unified recombination to the $3p$ and $3s$ states of Fe XVI may also be used to compare with the results in [10] along the same lines of approach in this paper for PR to the $3d$ states. However, due to the relatively large contributions from the background ions, such as Ar ions and Fe XVI (see [10] for more discussions on this point), the PR to the $3p$ and $3s$ states are not as clean as the PR to the $3d$ states if our major goal is to reanalyze the EBIT x-ray spectrum measured in [10] and to rederive the 3C and 3D EIE cross sections of Fe XVII.

IV. CONCLUSION

In conclusion, the major results we have obtained are the following: (1) We have carried out an elaborate and large-scale calculation for the photoionization processes of Fe XVI. The advanced BPRM method with 89 Fe XVII core states was included in the CC eigenfunction expansion. Prominent and complex resonance structures are demonstrated. (2) We have calculated the unified photorecombination processes (RR +DR) of Fe XVI from the BPRM photoionization cross sections via the generalized principle of detailed balance (the Milne relation). The DR cross sections and the interference of DR and RR are demonstrated to be important at low energy. (3) The effective photorecombination cross sections convolved with a Gaussian electron beam distribution are 24% higher than previous, less elaborate RHS RR calculation. The accuracy of the effective photorecombination cross sections in this work is estimated to be $\approx 5\%-10\%$ [21–23]. (4) The immediate consequence of the conclusion in (3) is that all the EIE cross sections derived in [10] for both the 3C and 3D lines should be raised by about 20%. This reduces significantly the puzzling large discrepancy (up to 50% or more) between previous theoretical Fe XVII 3C and 3D EIE cross sections and those derived from the EBIT x-ray spectrum in [10]. (5) The solution of the remaining 20%–30% discrepancy has already been given by the present author in a recent work on the converged EIE calculation of Fe XVII by using the fully relativistic close-coupling method [14].

ACKNOWLEDGMENTS

It is a pleasure for the author to thank the EBIT team members at NIST and CfA for stimulating discussions. The author is also grateful to K. Kirby, N. S. Brickhouse, and A. K. Pradhan for encouragement of the project. This work was supported by the NSF through a grant for the Institute for Theoretical Atomic, Molecular and Optical Physics at Harvard University and Smithsonian Astrophysical Observatory and in part by the Chandra X-ray Observatory (CXO) theory grant. All the computational work was carried out on the Cluster at the Computation Facility of CfA.

[1] D. E. Osterbrock, *Astrophysics of Gaseous Nebulae and Active Galactic Nuclei* (University Science Books, New York, 1989).
[2] T. R. Kallman and P. Palmeri, Rev. Mod. Phys. **79**, 79 (2007).
[3] M. D. Rosen *et al.*, Phys. Rev. Lett. **54**, 106 (1985); D. L. Matthews *et al.*, *ibid.* **54**, 110 (1985); T. N. Lee, E. A. McLean, and R. C. Elton, *ibid.* **59**, 1185 (1987).
[4] M. S. Turner *et al.*, *Connecting Quarks with the Cosmos* (National Academies Press, Washington, DC, 2003).
[5] G. X. Chen, K. Kirby, E. Silver, N. S. Brickhouse, J. D. Gillaspy, J. N. Tan, J. Pomeroy, and J. M. Laming, Phys. Rev. Lett. **97**, 143201 (2006).
[6] R. K. Smith, N. S. Brickhouse, D. A. Liedahl, and J. C. Raymond, Astrophys. J. **556**, L91 (2001).
[7] C. R. Canizares *et al.*, Astrophys. J. **539**, L41 (2000).
[8] J. N. Reeves *et al.*, Nature (London) **416**, 512 (2002); Y. Krongold *et al.*, Astrophys. J. **597**, 832 (2003).
[9] R. E. Marrs, M. A. Levine, D. A. Knapp, and J. R. Henderson, Phys. Rev. Lett. **60**, 1715 (1988); S. Chantrenne, P. Beiersdorfer, R. Cauble, and M. B. Schneider, *ibid.* **69**, 265 (1992).
[10] G. V. Brown *et al.*, Phys. Rev. Lett. **96**, 253201 (2006).
[11] B. W. Smith, J. C. Raymond, J. B. Mann, and R. D. Cowan, Astrophys. J. **298**, 898 (1985).
[12] G. V. Brown, P. Beiersdorfer, D. A. Liedahl, and K. Widmann, Astrophys. J. **502**, 1015 (1998).
[13] J. M. Laming *et al.*, Astrophys. J. **545**, L161 (2000).
[14] G. X. Chen, Phys. Rev. A **76**, 062708 (2007); *ibid.* **77**, 022701 (2008).
[15] G. X. Chen and A. K. Pradhan, Phys. Rev. Lett. **89**, 013202 (2002); G. X. Chen, A. K. Pradhan, and W. B. Eissner, J. Phys. B **36**, 453 (2003).
[16] J. H. Scofield, J. Electron Spectrosc. Relat. Phenom. **8**, 129 (1976). In the concluding paragraph of this paper, the author points out "The inaccuracy in the Hartree-Slater model in the treatment of the photoionization from isolated atoms comes

about because of the approximation manner of the treating the electron-electron interaction." The subshell photorecombination processes were calculated using the principle of detailed balance from the subshell photoionization processes (such as in [17]), so the subshell recombination rates reported in [17,10] should have the same limitation as the photoionization calculations by this Hartree-Slater model.

[17] J. H. Scofield, Phys. Rev. A **40**, 3054 (1989); E. B. Saloman, J. H. Hubbell, and J. H. Scofield, At. Data Nucl. Data Tables **38**, 1 (1988).

[18] K. A. Berrington, W. Eissner, and P. H. Norrington, Comput. Phys. Commun. **92**, 290 (1995); http://amdpp.phys.strath.ac.uk/UK_RmaX/codes.html

[19] D. Donnelly *et al.*, Astron. Astrophys. **349**, 996 (1999); M. K. Inal, A. Surzhykov, and S. Fritzsche, Phys. Rev. A **72**, 042720 (2005); J. J. Wan *et al.*, J. Phys.: Conf. Ser. **58**, 367 (2007).

[20] P. C. W. Davies and M. J. Seaton, J. Phys. B **2**, 757 (1969); R. H. Bell and M. J. Seaton, *ibid.* **18**, 1589 (1985).

[21] H. L. Zhang and A. K. Pradhan, Phys. Rev. Lett. **78**, 195 (1997); S. N. Nahar and A. K. Pradhan, *ibid.* **68**, 1488 (1992); A. K. Pradhan, *ibid.* **47**, 79 (1981).

[22] S. N. Nahar and A. K. Pradhan, Radiat. Phys. Chem. **70**, 323 (2004); H. L. Zhang, S. N. Nahar, and A. K. Pradhan, J. Phys. B **32**, 1459 (1999).

[23] A. K. Pradhan, G. X. Chen, S. N. Nahar, and H. L. Zhang, Phys. Rev. Lett. **87**, 183201 (2001).

[24] H. Chen *et al.*, Astrophys. J. **646**, 653 (2006).